

A Characteristic Signature of Magnetospheric Wave-Particle Interactions Found in the Turbulent E-region

Magnus F Ivarsen*

Department of Physics, University of Oslo, Oslo, Norway

Yukinaga Miyashita†

Space Science Division, Korea Astronomy and Space Science Institute, Daejeon, South Korea

Jean-Pierre St-Maurice,‡ Glenn C Hussey, Brian Pitzel, Draven Galeschuk, and Saif Marei
Department of Physics and Engineering Physics, University of Saskatchewan, Saskatoon, Canada

Richard B. Horne

British Antarctic Survey, Cambridge, UK

Yoshiya Kasahara and Shoya Matsuda

Graduate School of Natural Science and Technology, Kanazawa University, Kanazawa, Japan

Satoshi Kasahara and Kunihiro Keika

Department of Earth and Planetary Science, University of Tokyo, Tokyo, Japan

Yoshizumi Miyoshi, Kazuhiro Yamamoto, and Atsuki Shinbori

Institute for Space-Earth Environmental Research, Nagoya University, Nagoya, Japan

Devin R Huyghebaert§

Department of Physics and Technology, University of Tromsø, Tromsø, Norway

Ayako Matsuoka

Data Analysis Center for Geomagnetism and Space Magnetism, Kyoto University, Kyoto, Japan

Shoichiro Yokota

Department of Earth and Space Science, Osaka University, Toyonaka, Japan

Fuminori Tsuchiya

Planetary Plasma and Atmospheric Research Center, Tohoku University, Tohoku, Japan

(Dated: January 9, 2025)

Electromagnetic waves in the magnetosphere scatter electrons, causing them to precipitate deep into Earth's atmosphere, where they impart their temporal characteristics to diffuse aurorae. Using radar-observations of the ionospheric E-region and satellite observations from the magnetosphere, we demonstrate a close and unprecedented association between enhanced electrostatic cyclotron harmonic wave activity in the magnetosphere and the appearance of meter-scale ionospheric plasma turbulence observed a few seconds later in the lower ionosphere on nearby magnetic field lines.

INTRODUCTION

During major disturbances in geospace much energy is imparted from the solar wind to Earth's atmosphere. Large-scale electrical currents and the creation of strong electric fields at ionospheric altitudes ensues [1, 2]. The effect is widespread plasma turbulence [3, 4].

The ionosphere's the E-region (roughly the bottom-side) prominently features the Farley-Buneman (FB) instability [5, 6]. The intense meter-scale structures are excited when the relative drift (polarization electric field) between the strongly magnetized electrons and largely unmagnetized ions exceeds the local ion-acoustic speed

[7]. The requirement for a large relative drift means that the structures are found in Hall currents regions, the auroral electrojets. Radio signals that scatter off these waves have been coined the 'radar aurora' [8].

The ionosphere largely draws energy from diffuse aurorae at night [9, 10], produced when hot electrons near the ring current interact with naturally occurring waves through cyclotron resonance, causing pitch angle scattering and subsequent precipitation into the atmosphere [11–13]. Mechanisms notably include whistler-mode chorus and electrostatic cyclotron harmonic (ECH) waves [11, 14–17].

Recent advances have demonstrated that temporal os-

cillations in chorus wave activity are closely linked to the dynamic behaviour of pulsating aurorae [18–20]. This important discovery documents that the signature of *magnetospheric* processes can be reproduced in *ionospheric* processes.

The physical route for such processes to impact the ionosphere is twofold. First, the precipitating particles quasi-instantaneously introduce a perpendicular electric field. Second, local ionization of the plasma will modulate conductivities through chemistry with its fast increase in ion production rates courtesy of impacting particles recombining with the surrounding plasma, albeit in a somewhat more slowly pace [21].

Conjugate radar observations have established a firm link between auroral pulsations and electrodynamic oscillations in the ionosphere. Notably, periodic modulations in the plasma density, conductivity, and electric field strength are associated with pulsating aurorae [22, 23]. *In-situ* observations have revealed the presence of downward field-aligned (likely thermal) currents on the edges of such patches [24], and the filamentation (field-tube structuring) of those currents have been found to match the spatial signature of E-region plasma turbulence [25, 26].

Motivated by the above, we hypothesize that turbulent structuring of the electric and density fields in the auroral E-region are, at their core, *directly* caused by the wave-particle interactions in the diffuse aurora, with the aurora as a mediator of the driving signal. In testing this hypothesis, FB turbulence take center stage. Individual FB waves in the radar aurora are so intense and short-lived that they quickly dissipate and are replaced by new waves [27, 28]. When and where FB waves grow will thus depend on the spatio-temporal location of their sources, which, unequivocally, are aurorae [29].

DATA

To investigate whether magnetospheric wave activity can act as a direct driver of small-scale plasma turbulence in the ionosphere, we searched for space-ground conjunctions that took place when the Japanese inner-magnetosphere spacecraft Arase was close to magnetic equator, and with a northern hemisphere footprint that was within the field-of-view of the new Canadian ICEBEAR radar, and in the presence of active aurorae. Combining through coincident data collected between January 2020 and June 2023, we found one such event.

Figure 1a) shows an annotated optical image of diffuse, pulsating aurorae, taken with the TREX RGB system at Rabbit Lake [32]. The system was switched on at dusk, around midway into the event. Superposed on Figure 1a) is the point-cloud distribution of a few thousand ICEBEAR radar echoes detected in a 3-second interval following 06:56:45 UT on 12 May 2021. ICEBEAR is a coher-

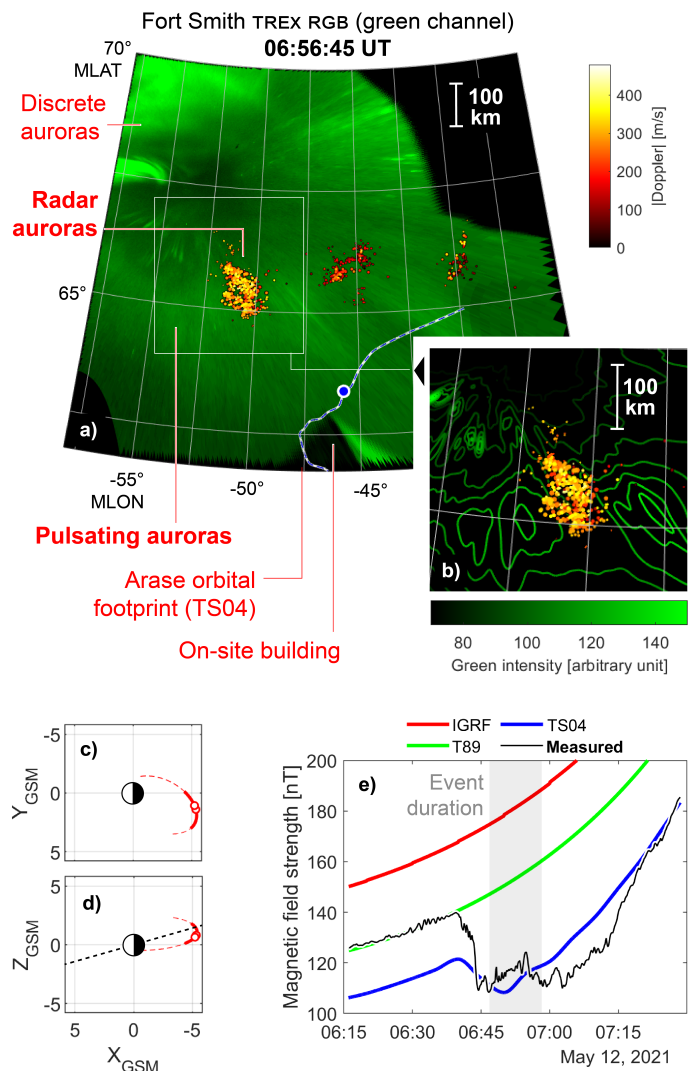


FIG. 1. A conjunction on 12 May 2021 between the ICEBEAR radar, a TREX auroral camera, and the ionospheric footprint of Arase. **Panels a–b)** show a 3-second auroral image (the green channel of the RGB-triplet) projected onto the ionosphere following Ref. [30], with the locations of radar echoes (color-coded according to Doppler shift), all shown in geomagnetic coordinates (AACGM, [31]). The ionospheric footprint of the magnetospheric spacecraft Arase is shown as a blue circle. An inset panel (b) enlarges a radar aurora shape that appears lodged between two pulsating patches (see also Video S2). **Panels c–d)** detail Arase’s journey in the magnetosphere in GSM coordinates, with magnetic equator appearing as a dashed black line (c–d). **Panel e)** compares the modeled (red, green, and blue) with the measured (black) magnetic field strength along Arase’s trajectory. See Figure 5 in the End Matter for a graphical representation.

ent scatter radar that combines multiple interferometry links with a coded pseudo-random continuous-wave signal to achieve high resolution 3D radar data in time and space [33, 34].

In Figure 1a), and in Videos S1 and S2 in the supplementary data, the radar echoes cluster between evol-

ing pulsating auroral patches along their poleward flank, where electric field enhancements maximize [23]; this is contrary to the patches' interiors, where elevated conductivities may short out the field entirely [24, 35]. Each received echo indicates the presence of turbulent electrojet currents in the space around the pulsating patches.

The direct cause of these turbulent currents were observed by Arase in the distant equatorial magnetosphere. Arase's orbit during the event is shown in Figure 1c–d); it has an apogee of 32,000 km and a perigee of 400 km, an inclination angle of 31° , and an orbital period of 570 minutes [36]. Figure 1e) substantiates the relative accuracy of the TS04 model [37] in mapping Arase's magnetic footprint from its orbit down to the northern hemisphere E-region, a mapping that is in general made uncertain by Alfvén waves and field-aligned currents [38]. Arase's footprint is estimated to lie on the equatorward flank of the pulsating aurorae, whose poleward flank is occupied by radar echoes.

The magnetospheric measurements used in the present letter are summarized in Figure 2. We analyze mostly electric field power spectra on frequencies between 0.1 kHz and 20 kHz, a range in which whistler-mode chorus waves and electrostatic cyclotron harmonic waves often appear. The measurements originate in the Plasma wave experiment (PWE) instrument onboard Arase. The data product consists of electric field power spectrograms [39, 40], shown in Figure 2a). In addition to wave power, we also collected data from Arase's onboard Medium-energy particle detector (MEP-e), which detects 7 keV to 87 keV precipitating electrons [41], shown in Figure 2b). Lastly, Figure 2c) shows the auroral electrojet index (SME-index, black line, left axis), and the SymH-index (red line, right axis).

Geospace description

We are now in a position to formulate and interpret the conditions of geospace during our event. The conjunction, which was preceded by a geomagnetically quiet period, took place during drastic and coincident increases in the SME- and SymH-indices. The strong impulse in these indices was the effect of a sudden nine-fold jump in solar wind dynamic pressure (not shown), which led to magnetospheric compression [42].

Around 06:40 UT, Arase, situated at the equator (-1° MLAT), suddenly found itself outside the plasmasphere, witnessed by the rapid decrease in the upper hybrid resonance frequency (f_{UHR} in Figure 2a, [43]). Arase was thus experiencing optimal conditions for the observation of ECH waves [44, 45], waves that were simultaneously given access to hot ring current electrons [46]. The loss of these electrons into Earth's atmosphere resulted in the diffuse aurorae observed with the TREX RGB system in Figure 1a–b) and in Video S2.

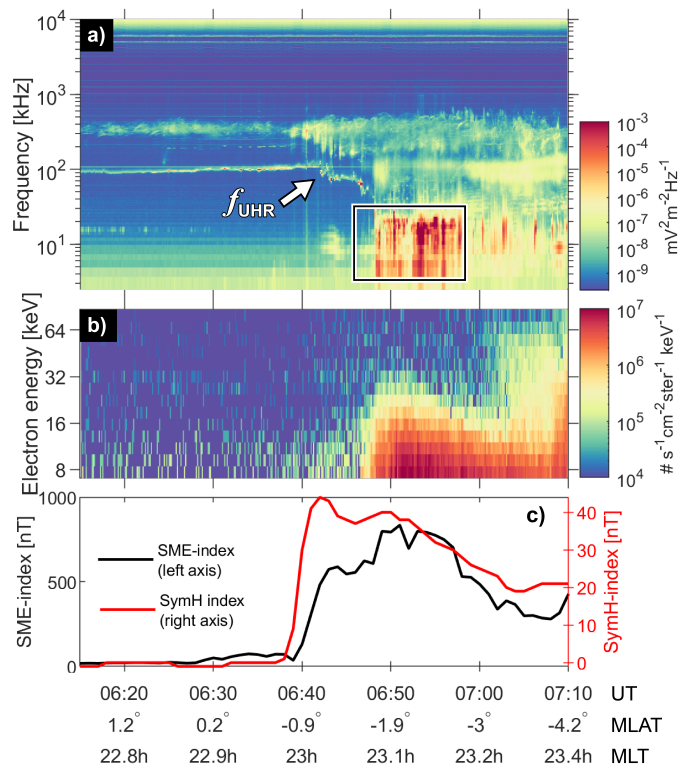


FIG. 2. **Panel a):** High-frequency electric field spectrogram from Arase's PWE instrument. The black rectangle refers to the analysis in Figure 3). **Panel b):** precipitating electron energy flux from Arase's medium-energy particle detector (the low-energy detector data was unavailable). The data shows pitch angles lower than 10° , but we additionally confirmed that it was consistent with the parallel-flux data (pitch angles $< 2^\circ$). **Panel d):** The SME-index (left axis) and the SymH-index (right axis). The three x -axes show time in UT (on 12 May 2021), and Arase's orbital location in the magnetosphere.

Penetrating electric fields

Next, we shall compare the wave power measured by Arase with the FB turbulence echo *detection rates* measured by the ICEBEAR radar, the rate at which ICEBEAR's range and Doppler gates are receiving signals. That metric is exceedingly simple: it entails counting the raw number of radar echoes detected for each timestep (1 s). With the premise of extant FB waves being ephemeral, changes in this metric will reflect changes in the turbulent driver within ICEBEAR's field-of-view.

Figure 3a) shows wave power at 1 second cadence [47], encompassing the interval 06:46:00 UT – 06:58:30 UT, and highlighting three frequencies with dashed black lines ($0.5f_e$, f_e , and $2f_e$, with f_e being the local electron cyclotron frequency, calculated using the DC magnetic field data from the MGF instrument [48]). Figure 3b) uses a solid red line to show the integrated power (referred to as RMS, or root-mean-square) in the $f > 2f_e$ range, and we now superpose the ICEBEAR echo detection rate with

a solid black line (right axis). Figure 3c) shows the result of a cross-correlation analysis performed between the echo detection rates and the wave power RMS in four frequency ranges. For the $f > 2f_e$ range, we observe strong correlation (Pearson coefficient $\rho = 0.82$, shown in Panel d), with a peak lag of 7 seconds, indicating that optimal correlation is obtained by shifting the Arase-observations 7 seconds back in time. This lag should be compared to the time-of-flight for the electrons of around 1 s [49, 50], and we note that the correlation is similar for a 1 s lag. Figure 3e) shows explicitly how this result depends on frequency. It shows a cross-correlation analysis on a moving window both in time and frequency. There is a noticeable uptick in correlation at $f = 2f_e$ and at $f = 4f_e$ the correlation coefficient reaches 0.94. We note that this latter correlation were determined at a zero-lag (< 1 second), on the order of the time-of-flight of the electrons themselves. The p -values (probabilities that the correlations were spurious) obtained for the two quoted coefficients were zero at floating point precision.

Ionization in the Lower Ionosphere

Having demonstrated a close correspondence between the evolution of ECH wave power and that of turbulence echo detection rate, we shall next demonstrate a link between the evolution of the particle flux at Arase's orbit, and that of the echo detection *altitudes*. Figure 4a) plots the 8 keV–87 keV-electron energy flux. We then assume the flux is a proxy for the real precipitating energy flux, treating it as 16 mono-energetic beams of electrons (one for each energy channel). We apply the parameterizations in Ref. [51] to estimate ionization altitude profile for beam of electrons. The cumulative profile then corresponds to the emission altitude profile of the aurora.

The results of this altitude analysis are shown in Figure 4c–d), where we likewise plot the total altitude distribution of the radar echo point cloud. The two timeseries in Figure 4c) exhibit a Pearson correlation coefficient of 0.87, and the two profiles in Figure 4d) match surprisingly well, with peaks in the distributions being separated by only 1.5 km. The unambiguous similarity points to a causal link between the particle-induced ionization and the distribution of radar echoes in the E-region.

DISCUSSION

At the event's onset, Arase had just exited the plasmasphere at the equator (orbiting from -1.5° to -3° MLAT) where it observed intense ($0.1 \text{ mV}^{-2}\text{m}^{-1}$) ECH waves inside the region where such waves are confined [44, 45], and capable of accelerating keV-electrons towards Earth's atmosphere [14, 17, 44, 52].

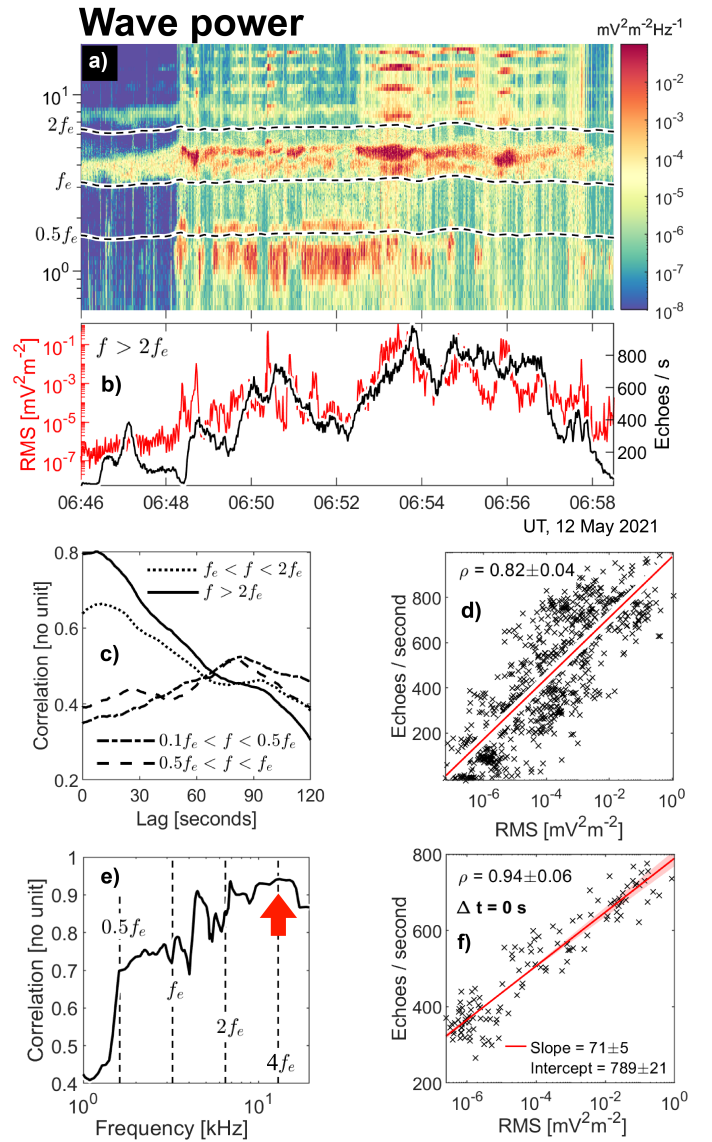


FIG. 3. **panel a)**: Electric field spectrogram observed between 06:46:00 UT and 06:58:30 UT on 12 May 2021, with three frequencies indicated ($0.5f_e$, f_e , and $2f_e$). **Panel b)**: RMS for the $2f_e < f < 19.45$ kHz frequency range, with the ICEBEAR echo detection rate superposed (right axes). **Panel c)**: cross-correlation analysis between the echo rates and the RMS for all four frequency ranges. **Panel d)**: scatterplot of the data in panel b), with the ECH wave power having been shifted 7 seconds back in time; Pearson correlation coefficient for a log-linear fit, with an error margin given by 95-percent (3-sigma) confidence intervals is indicated. **Panel e)**: the highest cross-correlation obtained from a moving window in frequency (7 logarithmic increments out of 132) and time (2 minutes), with a maximum allowed lag of 9 seconds. **Panel f)**: scatterplot akin to Panel d), but for frequencies around $4f_e$ ($11.5 \text{ kHz} < f < 15 \text{ kHz}$), during a 2-minute window centered on 06:52:32 UT (at zero lag). A near-perfect correlation is posted.

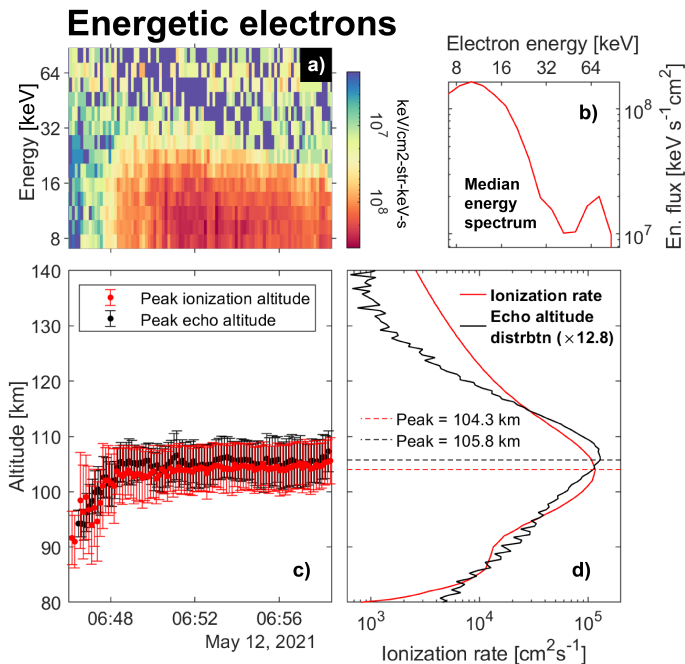


FIG. 4. **Panel a)**: Precipitating particle energy flux measured by Arase. **Panel b)**: Median energy spectrum. **Panel c)**: ICEBEAR echo altitudes as a function of time (black dots) and the peak emission altitude based on the electron energy flux (red errorbars), using generalized parametrization of numerical models [51], including the MSIS model of Earth’s atmosphere [53]. **Panel d)**: overall ICEBEAR echo altitude distribution (black) and auroral emission altitude profile (red), peak altitudes indicated.

Arase’s footprint in the ionosphere was likely 100 – 200 kilometers south of the echo region, with diffuse auroral shapes appearing in between. The precipitating electrons inside the patches briefly accumulated at an altitude of around 104 km and produced there strong electric fields [54, 55] and plasma density gradients by merit of ionizing the gas. The plasma becomes gradient drift unstable [56], and at the same time, the Farley-Buneman instability may saturate [57]. Once saturated the instability produces secondary waves [58, 59] and dissipate the wave power through heating [60, 61]. The high-amplitude FB waves dissipate fast, giving the turbulence the impression of being ephemeral, or instantaneous, [62]. Ultimately, this allows the ensemble radio echoes from those waves to accurately reflect the changes in the instability driver on timescales larger than a second, facilitating the strong correlations in Figure 3d–f) as well as the co-evolution of the timeseries in Figure 4c).

The resulting image is one of a self-similar and simultaneous, turbulent state at points in space separated by 5 Earth radii, and indicates that the entire turbulent process retains a distinct ‘stochastic shape’ that is conserved down to meter-scale.

There is a causal and largely instantaneous path from

the modulation of ECH waves to small-scale turbulence. It involves particle precipitation, which creates beams of electrons that modulate conductivity (ionization) and electric fields [63]. Those modulations produce gradient-drift unstable structures [56], whose imminent decay into smaller and smaller pieces, the turbulent cascade, systematically breaks apart structures smaller in size than around 1–10 km [64, 65]. The shapes, or rather, their stochastic features, are subsequently repeated in a self-similar pattern that reaches as small as meter-scale in magnification, at which point the initial perturbations will have seeded the Farley-Buneman instability and saturating its growth rates (see Figure 5 for a schematic illustration of this cascading process).

Other driving mechanisms are readily available, such as Alfvén waves and other field-parallel acceleration mechanisms, as well as magnetospheric ion cyclotron waves, and other wave-particle interactions. However, as shown by Figure 3d–f), the ensemble of radar echoes recreate temporal changes in the magnetospheric wave-particle interactions with remarkable fidelity: the production of small-scale plasma turbulence identifies its maker, faithfully mimicking its driving signal, ostensibly by *dissipating* that signal.

Refreshingly and for a brief moment, then, the local space weather had a clear physical driver. The turbulent transformation of this driving signal can inform development of models that aim to predict the occurrence of plasma turbulence around aurorae.

SUMMARY

In this letter, we have reported a conjunction between Arase’s northern hemisphere footprint and the ICEBEAR radar’s field-of-view. Arase observed strong electrostatic cyclotron harmonic wave activity at the magnetic equator. On a nearby magnetic field line, ICEBEAR recorded a matching radar signal from turbulent electrojets in the space between pulsating aurorae.

Our interpretation of the findings, and the only viable explanation for their cause, is that an ensemble of wave-particle interactions imparted their temporal and spatial characteristics to a spatio-temporal pattern of electron precipitation. The electrons inside these structures produced pulsating aurorae and introduced an associated pattern of ionization and electric field enhancements in the E-region that were insensibly picked up by the growth of FB waves. The growth, saturation, and subsequent detection of these waves faithfully reflected the evolution of the underlying driver.

We conclude that the detection of small-scale plasma turbulence in the auroral E-region can be applied as a diagnostic tool to quantify the whole energy input behind space weather events, a remarkable victory for the concept of mode-coupling in plasma physics.

END MATTER

A Graphic Representation of the Findings

Figure 5a) illustrates the electrodynamics of the conjugate measurements analyzed in the present letter. Intense electric fields, which point in the course taken by moving ions, are organized in some pattern outside of pulsating auroral patches [23]. The field points away from downwards (likely thermal) currents and towards the upwards currents (aurorae). Surrounding the pulsating patches are plasma density gradients [22].

Figure 5b–d) illustrate how this description turns into turbulent energy dissipation, as the density structures in Panel a) become gradient-drift unstable [66]. The resulting waves decay into smaller-and-smaller turbulent branches, eventually acting as seeds for the meter-scale Farley-Buneman instability. Thus, a turbulent signal is formed by *the ensemble* of 3-meter Farley-Buneman waves, one whose temporal characteristics approach that of the wave power, the underlying driver.

The Measurement locations of those two matching turbulent signals are indicated around the pulsating patches in the electrodynamic diagram in Figure 5a), and Figure 5b–c) illustrate the turbulent signal formation in the lower ionosphere.

Part of a Trend?

We argue that the clear-cut event analyzed in the present letter is not a one-off, but rather part of a trend, where Ref. [67] presents relevant evidence from the day-side polar ionosphere. Indeed, the turbulent Hall channels that may frequent the vicinity of diffuse aurorae in general are highly localized in time and space, like most research into the “spiky” nature of electric field enhancements can attest [54]. To support such a general connection between magnetospheric wave-particle energy and subsequent modulations to the ICEBEAR echo detection rates, we have fallen back on inferences made from statistics.

We aggregated the echo detection rates between magnetic local times of 20h and 06h, a distribution that is roughly consistent with surveys of ECH waves [44, 45]. We took the raw number of echoes per second after removing bins with a mean signal-to-noise ratio lower than 1.5, which removes the occasional radio interference, and discarding bins in which only a single echo was detected. We subsequently aggregated Arase ECH wave power RMS for frequencies $f > 2f_e$, when the satellite was within 5° of the equator at the same magnetic local time interval, and with a northern hemisphere orbital footprint between 60° and 72° MLAT.

In Figure 6a–b) we show the resulting median values for the echo detection rates and wave power respectively,

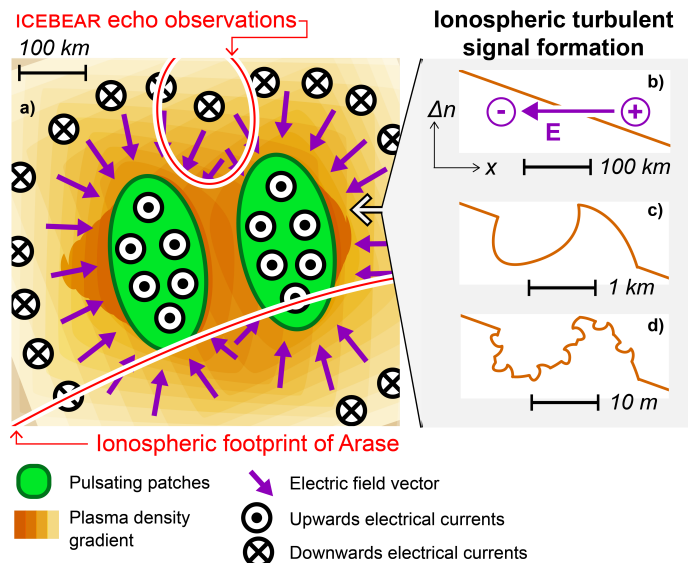


FIG. 5. **Panel a):** Annotated schematic depiction of the the electrodynamics surrounding the ICEBEAR and Arase measurements. **Panel b):** A schematic representation of a density structure near one of the pulsating patches in panel a), along the density gradient (Δn), and with an applied electric field (E). Together these generate sub-kilometer-scale turbulent structures through the gradient drift instability. The irregular structures further decay into smaller-and-smaller pieces, eventually seeding the 3-meter-sized Farley-Buneman instability, itself likewise triggered by E . Panels b–d) are each $100\times$ magnifications of the foregoing panel.

in 15 geomagnetic activity bins. In Panel a) we observe a distinct kink in the curve at an SME-index value of around 150 nT, below which the echo detection rate is flat (indicating a contamination by meteor trail echoes [68]). For bins above this kink, the bin-median echo detection rate is perfectly correlated ($\rho = 1$) with the SME-index. Crucially, the linear slope (1.71 ± 0.11 in a log-log scale) is roughly consistent with the slope exhibited by the wave power data (Figure 6b), 2.23 ± 0.31 .

The two quantities exhibit a similar response to enhancements in the SME-index. This facilitates the 1:1 relationship shown in Figure 6c), where we display the same geomagnetic activity bins in a scatterplot (excluding the gray datapoints in Panel a), and a log-log linear fit with slope 1 is shown with a red, dashed line. Lastly, with a green-blue circle, we show the median values derived from the 12 May 2021 event, with errorbars denoting upper/lower quartile distributions.

Figure 6a–b) show two widely different geophysical quantities – one in the ionosphere and one in the magnetosphere – that nevertheless respond in a similar fashion to a *third* independent variable, the SME-index. Indeed, that index is itself an unambiguous measurement from the ground of the ionosphere’s high-latitude Hall currents (the auroral electrojets) [69, 70]. Enhancements in Hall conductance are, in turn, driven by energetic particle pre-

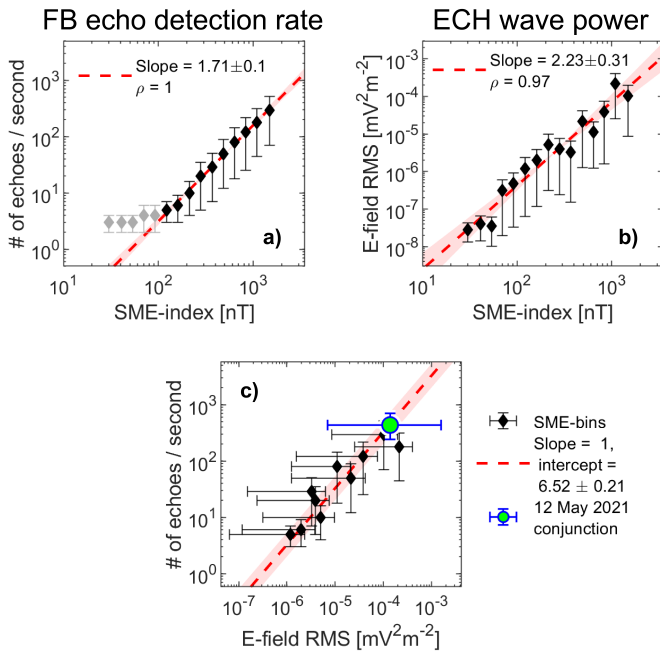


FIG. 6. The ICEBEAR echo detection rate, for some 1.2 million one-second intervals (containing a total of 272 million echoes) (**Panel a**), and the Arase-observed wave RMS ($f > 2f_c$) for some 530,000 one-second wave spectra (**Panel b**). Black diamonds represent the median value of 15 logarithmically spaced SME-index bins, and vertical errorbars denote upper/lower quartile distributions. Linear fits are indicated, by non-linear least squares minimization of the root-mean-square error, and error margins are posted showing 95-percent confidence intervals of the fits (3-sigma). **Panel c** shows the same bins in a scatterplot, with a red dashed line denoting a 1:1 relation. The data was collected between January 2020 and June 2023 during days when the radar was operational. Data from the 12 May 2021 event is shown with a green circle.

precipitation [71, 72], by virtue of providing ionization and driving electric field enhancements. As we detail above (and illustrate in Figure 5), the same two quantities ultimately drive Farley-Buneman turbulence.

In empirical terms, the diffuse and pulsating aurorae constitute the majority of the total energy input into the nightside ionosphere [73], and so enhancements in the Hall currents are largely driven by diffuse and pulsating aurorae [22, 74]. There, ECH waves constitute a vital part of the acceleration mechanisms [11, 17, 44, 50].

The ICEBEAR echo rate reflects the amplitude and spatial extent of any large-amplitude meter-scale Farley-Buneman-generated turbulence in the electrojets within the radar field-of-view [75–77].

The above chain of argument explains why the SME-index is, on average, perfectly correlated with ICEBEAR’s echo count. The SME-index is a global quantity, and so the echo count is not expected to track it during individual events. The average number of echoes per time-interval will, given a large enough sample, be perfectly correlated with the SME-index.

ACKNOWLEDGEMENTS

This work is supported in part by Research Council of Norway (RCN) grant [324859]. We acknowledge the support of the Canadian Space Agency (CSA) [20SUGOICEB], the Canada Foundation for Innovation (CFI) John R. Evans Leaders Fund [32117], the Natural Science and Engineering Research Council (NSERC), the Discovery grants program [RGPIN-2019-19135], the Digital Research Alliance of Canada [RRG-4802], and basic research funding from Korea Astronomy and Space Science Institute [KASI2024185002]. Science data of the ERG (Arase) satellite were obtained from the ERG Science Center operated by ISAS/JAXA and ISEE/Nagoya University (<https://ergsc.isee.nagoya-u.ac.jp/index.shtml.en>). This includes Lv.3 MEP-e (DOI 10.34515/DATA.ERG-02003), Lv.2 PWE/OFA (DOI 10.34515/DATA.ERG-08000), Lv.2 PWE/HFA (DOI 10.34515/DATA.ERG-10000), and Lv.2 MGF (DOI 10.34515/DATA.ERG-06001). ICEBEAR 3D echo data for 2020, 2021 is published with DOI 10.5281/zenodo.7509022. SuperMAG data can be accessed at <https://supermag.jhuapl.edu/mag/>. The SymH-index from NASA’s OMNI service can be accessed at <https://omniweb.gsfc.nasa.gov/>. TREX optical data can be accessed at <https://data.phys.ucalgary.ca/> [78]. MFI is thankful to F Lind, Y Jin, W Miloch, and L Clausen for stimulating discussions.

* Now at Department of Physics and Engineering Physics, University of Saskatchewan, Saskatoon, Canada

† Also at Department of Astronomy and Space Science, Korea University of Science and Technology, Daejeon, South Korea

‡ Also at Department of Physics and Astronomy, University of Western Ontario, London, Canada

§ Also at Department of Physics and Engineering Physics, University of Saskatchewan, Saskatoon, Canada

- [1] T. Iijima and T. A. Potemra, Large-scale characteristics of field-aligned currents associated with substorms, *Journal of Geophysical Research: Space Physics* **83**, 599 (1978).
- [2] A. Keiling, S. Thaller, J. Wygant, and J. Dombek, Assessing the global Alfvén wave power flow into and out of the auroral acceleration region during geomagnetic storms, *Science Advances* **5**, eaav8411 (2019).
- [3] J. D. Huba, A. B. Hassam, I. B. Schwartz, and M. J. Keiskinen, Ionospheric turbulence: Interchange instabilities and chaotic fluid behavior, *Geophysical Research Letters* **12**, 65 (1985).
- [4] M. Wiltberger, V. Merkin, B. Zhang, F. Toffoletto, M. Oppenheim, W. Wang, J. G. Lyon, J. Liu, Y. Dimant, M. I. Sitnov, and G. K. Stephens, Effects of electrojet turbulence on a magnetosphere-ionosphere simulation of a geomagnetic storm, *Journal of Geophysical Research: Space Physics* **122**, 5008 (2017).

- [5] D. T. Farley, A plasma instability resulting in field-aligned irregularities in the ionosphere, *Journal of Geophysical Research* (1896-1977) **68**, 6083 (1963).
- [6] O. Buneman, Excitation of Field Aligned Sound Waves by Electron Streams, *Physical Review Letters* **10**, 285 (1963).
- [7] M. M. Oppenheim and Y. S. Dimant, Kinetic simulations of 3-D Farley-Buneman turbulence and anomalous electron heating, *Journal of Geophysical Research: Space Physics* **118**, 1306 (2013).
- [8] D. L. Hysell, The Radar Aurora, in *Auroral Dynamics and Space Weather* (American Geophysical Union (AGU), 2015) Chap. 14, pp. 191–209.
- [9] P. T. Newell, T. Sotirelis, and S. Wing, Seasonal variations in diffuse, monoenergetic, and broadband aurora, *Journal of Geophysical Research: Space Physics* **115**, 10.1029/2009JA014805 (2010).
- [10] R. M. Robinson, R. R. Vondrak, K. Miller, T. Dabbs, and D. Hardy, On calculating ionospheric conductances from the flux and energy of precipitating electrons, *Journal of Geophysical Research: Space Physics* **92**, 2565 (1987).
- [11] B. Ni, R. M. Thorne, Y. Y. Shprits, and J. Bortnik, Resonant scattering of plasma sheet electrons by whistler-mode chorus: Contribution to diffuse auroral precipitation, *Geophysical Research Letters* **35**, 10.1029/2008GL034032 (2008).
- [12] J. Birn, A. V. Artemyev, D. N. Baker, M. Echim, M. Hoshino, and L. M. Zelenyi, Particle Acceleration in the Magnetotail and Aurora, *Space Science Reviews* **173**, 49 (2012).
- [13] B. Ni, J. Bortnik, Y. Nishimura, R. M. Thorne, W. Li, V. Angelopoulos, Y. Ebihara, and A. T. Weatherwax, Chorus wave scattering responsible for the Earth's day-side diffuse auroral precipitation: A detailed case study, *Journal of Geophysical Research: Space Physics* **119**, 897 (2014).
- [14] R. B. Horne, R. M. Thorne, N. P. Meredith, and R. R. Anderson, Diffuse auroral electron scattering by electron cyclotron harmonic and whistler mode waves during an isolated substorm, *Journal of Geophysical Research: Space Physics* **108**, 10.1029/2002JA009736 (2003).
- [15] J. Liang, V. Uritsky, E. Donovan, B. Ni, E. Spanswick, T. Trondsen, J. Bonnell, A. Roux, U. Auster, and D. Larson, THEMIS observations of electron cyclotron harmonic emissions, ULF waves, and pulsating auroras, *Journal of Geophysical Research: Space Physics* **115**, 10.1029/2009JA015148 (2010).
- [16] B. Ni, J. Liang, R. M. Thorne, V. Angelopoulos, R. B. Horne, M. Kubyshkina, E. Spanswick, E. F. Donovan, and D. Lummerzheim, Efficient diffuse auroral electron scattering by electrostatic electron cyclotron harmonic waves in the outer magnetosphere: A detailed case study, *Journal of Geophysical Research: Space Physics* **117**, 10.1029/2011JA017095 (2012).
- [17] S. Kurita, Y. Miyoshi, C. M. Cully, V. Angelopoulos, O. L. Contel, M. Hikishima, and H. Misawa, Observational evidence of electron pitch angle scattering driven by ECH waves, *Geophysical Research Letters* **41**, 8076 (2014).
- [18] S. Kasahara, Y. Miyoshi, S. Yokota, T. Mitani, Y. Kasahara, S. Matsuda, A. Kumamoto, A. Matsuoka, Y. Kazama, H. U. Frey, V. Angelopoulos, S. Kurita, K. Keika, K. Seki, and I. Shinohara, Pulsating aurora from electron scattering by chorus waves, *Nature* **554**, 337 (2018).
- [19] K. Hosokawa, Y. Miyoshi, M. Ozaki, S.-I. Oyama, Y. Ogawa, S. Kurita, Y. Kasahara, Y. Kasaba, S. Yagitani, S. Matsuda, F. Tsuchiya, A. Kumamoto, R. Kataoka, K. Shiokawa, T. Raita, E. Turunen, T. Takashima, I. Shinohara, and R. Fujii, Multiple time-scale beats in aurora: Precise orchestration via magnetospheric chorus waves, *Scientific Reports* **10**, 3380 (2020).
- [20] Y. Miyoshi, K. Hosokawa, S. Kurita, S.-I. Oyama, Y. Ogawa, S. Saito, I. Shinohara, A. Kero, E. Turunen, P. T. Verronen, S. Kasahara, S. Yokota, T. Mitani, T. Takashima, N. Higashio, Y. Kasahara, S. Matsuda, F. Tsuchiya, A. Kumamoto, A. Matsuoka, T. Hori, K. Keika, M. Shoji, M. Teramoto, S. Imajo, C. Jun, and S. Nakamura, Penetration of MeV electrons into the mesosphere accompanying pulsating aurorae, *Scientific Reports* **11**, 13724 (2021).
- [21] R. W. Schunk and J. J. Sojka, A theoretical study of the lifetime and transport of large ionospheric density structures, *Journal of Geophysical Research: Space Physics* **92**, 12343 (1987).
- [22] K. Hosokawa, Y. Ogawa, A. Kadokura, H. Miyaoka, and N. Sato, Modulation of ionospheric conductance and electric field associated with pulsating aurora, *Journal of Geophysical Research: Space Physics* **115**, 10.1029/2009JA014683 (2010).
- [23] K. Hosokawa, T. Motoba, A. S. Yukimatu, S. E. Milan, M. Lester, A. Kadokura, N. Sato, and G. Bjornsson, Plasma irregularities adjacent to auroral patches in the postmidnight sector, *Journal of Geophysical Research: Space Physics* **115**, 10.1029/2010JA015319 (2010).
- [24] D. M. Gillies, D. Knudsen, E. Spanswick, E. Donovan, J. Burchill, and M. Patrick, Swarm observations of field-aligned currents associated with pulsating auroral patches, *Journal of Geophysical Research: Space Physics* **120**, 9484 (2015).
- [25] M. F. Ivarsen, A. Lozinsky, J.-P. St-Maurice, A. Spicher, D. Huyghebaert, G. C. Hussey, D. Galeschuk, B. Pitzel, and J. Vierinen, The Distribution of Small-Scale Irregularities in the E-Region, and Its Tendency to Match the Spectrum of Field-Aligned Current Structures in the F-Region, *Journal of Geophysical Research: Space Physics* **128**, e2022JA031233 (2023).
- [26] M. F. Ivarsen, M. D. Gillies, D. R. Huyghebaert, J.-P. St-Maurice, A. Lozinsky, D. Galeschuk, E. Donovan, and G. C. Hussey, Turbulence Embedded Into the Ionosphere by Electromagnetic Waves, *Journal of Geophysical Research: Space Physics* **129**, e2023JA032310 (2024).
- [27] P. Prikryl, D. André, G. J. Sofko, and J. A. Koehler, Doppler radar observations of harmonics of electrostatic ion cyclotron waves in the auroral ionosphere, *Journal of Geophysical Research: Space Physics* **93**, 7409 (1988).
- [28] P. Prikryl, D. Andre, J. A. Koehler, G. J. Sofko, and M. J. McKibben, Evidence of highly localized auroral scatterers from 50-MHz CW radar interferometry, *Planetary and space science* **38**, 933 (1990).
- [29] M. F. Ivarsen, D. R. Huyghebaert, M. D. Gillies, J.-P. St-Maurice, D. R. Themens, M. Oppenheim, B. J. Gustavsson, D. Billett, B. Pitzel, D. Galeschuk, E. Donovan, and G. C. Hussey, Turbulence Around Auroral Arcs, *Journal of Geophysical Research: Space Physics* **129**, e2023JA032309 (2024).
- [30] D. M. Gillies, J. Liang, E. Donovan, and E. Spanswick, The Apparent Motion of STEVE and the Picket

- Fence Phenomena, *Geophysical Research Letters* **47**, e2020GL088980 (2020).
- [31] S. G. Shepherd, Altitude-adjusted corrected geomagnetic coordinates: Definition and functional approximations, *Journal of Geophysical Research: Space Physics* **119**, 7501 (2014).
- [32] D. M. Gillies, E. Donovan, D. Hampton, J. Liang, M. Connors, Y. Nishimura, B. Gallardo-Lacourt, and E. Spanswick, First Observations From the TReX Spectrograph: The Optical Spectrum of STEVE and the Picket Fence Phenomena, *Geophysical Research Letters* **46**, 7207 (2019).
- [33] D. Huyghebaert, G. Hussey, J. Vierinen, K. McWilliams, and J.-P. St-Maurice, ICEBEAR: An all-digital bistatic coded continuous-wave radar for studies of the E region of the ionosphere, *Radio Science* **54**, 349 (2019).
- [34] A. Lozinsky, G. Hussey, K. McWilliams, D. Huyghebaert, and D. Galeschuk, ICEBEAR-3D: A Low Elevation Imaging Radar Using a Non-Uniform Coplanar Receiver Array for E Region Observations, *Radio Science* **57**, e2021RS007358 (2022).
- [35] N. C. Maynard, A. Bahnsen, P. Christophersen, A. Ege-land, and R. Lundin, An example of anticorrelation of auroral particles and electric fields, *J. Geophys. Res.*, v. 78, no. 19, pp. 3976-3980 10.1029/JA078i019p03976 (1973).
- [36] Y. Miyoshi, I. Shinohara, T. Takashima, K. Asamura, N. Higashio, T. Mitani, S. Kasahara, S. Yokota, Y. Kazama, S.-Y. Wang, S. W. Y. Tam, P. T. P. Ho, Y. Kasahara, Y. Kasaba, S. Yagitani, A. Matsuoka, H. Kojima, Y. Katoh, K. Shiokawa, and K. Seki, Geospace exploration project ERG, *Earth, Planets and Space* **70**, 101 (2018).
- [37] N. A. Tsyganenko and M. I. Sitnov, Modeling the dynamics of the inner magnetosphere during strong geomagnetic storms, *Journal of Geophysical Research: Space Physics* **110**, 2004JA010798 (2005).
- [38] J. E. Borovsky and J. Bonnell, The dc electrical coupling of flow vortices and flow channels in the magnetosphere to the resistive ionosphere, *Journal of Geophysical Research: Space Physics* **106**, 28967 (2001).
- [39] Y. Kasahara, Y. Kasaba, H. Kojima, S. Yagitani, K. Ishisaka, A. Kumamoto, F. Tsuchiya, M. Ozaki, S. Matsuda, T. Imachi, Y. Miyoshi, M. Hikishima, Y. Katoh, M. Ota, M. Shoji, A. Matsuoka, and I. Shinohara, The Plasma Wave Experiment (PWE) on board the Arase (ERG) satellite, *Earth, Planets and Space* **70**, 86 (2018).
- [40] A. Kumamoto, F. Tsuchiya, Y. Kasahara, Y. Kasaba, H. Kojima, S. Yagitani, K. Ishisaka, T. Imachi, M. Ozaki, S. Matsuda, M. Shoji, A. Matsuoka, Y. Katoh, Y. Miyoshi, and T. Obara, High Frequency Analyzer (HFA) of Plasma Wave Experiment (PWE) onboard the Arase spacecraft, *Earth, Planets and Space* **70**, 82 (2018).
- [41] S. Kasahara, S. Yokota, T. Mitani, K. Asamura, M. Hirahara, Y. Shibano, and T. Takashima, Medium-energy particle experiments—electron analyzer (MEP-e) for the exploration of energization and radiation in geospace (ERG) mission, *Earth, Planets and Space* **70**, 69 (2018).
- [42] Q. Q. Shi, X.-C. Shen, A. M. Tian, A. W. Degeling, Q. Zong, S. Y. Fu, Z. Y. Pu, H. Y. Zhao, H. Zhang, and S. T. Yao, Magnetosphere Response to Solar Wind Dynamic Pressure Change, in *Dayside Magnetosphere Interactions* (American Geophysical Union (AGU), 2020) Chap. 5, pp. 77–97.
- [43] Y. Miyoshi, A. Morioka, H. Misawa, T. Obara, T. Nagai, and Y. Kasahara, Rebuilding process of the outer radiation belt during the 3 November 1993 magnetic storm: NOAA and Exos-D observations, *Journal of Geophysical Research: Space Physics* **108**, SMP 3 (2003).
- [44] N. P. Meredith, R. B. Horne, R. M. Thorne, and R. R. Anderson, Survey of upper band chorus and ECH waves: Implications for the diffuse aurora, *Journal of Geophysical Research: Space Physics* **114**, 10.1029/2009JA014230 (2009).
- [45] B. Ni, R. M. Thorne, N. P. Meredith, R. B. Horne, and Y. Y. Shprits, Resonant scattering of plasma sheet electrons leading to diffuse auroral precipitation: 2. Evaluation for whistler mode chorus waves, *Journal of Geophysical Research: Space Physics* **116**, 10.1029/2010JA016233 (2011).
- [46] B. H. Ahn, H. W. Kroehl, Y. Kamide, D. J. Gorney, S. I. Akasofu, and J. R. Kan, The auroral energy deposition over the polar ionosphere during substorms, *Planetary and Space Science* **37**, 239 (1989).
- [47] S. Matsuda, Y. Kasahara, H. Kojima, Y. Kasaba, S. Yagitani, M. Ozaki, T. Imachi, K. Ishisaka, A. Kumamoto, F. Tsuchiya, M. Ota, S. Kurita, Y. Miyoshi, M. Hikishima, A. Matsuoka, and I. Shinohara, Onboard software of Plasma Wave Experiment aboard Arase: Instrument management and signal processing of Waveform Capture/Onboard Frequency Analyzer, *Earth, Planets and Space* **70**, 75 (2018).
- [48] A. Matsuoka, M. Teramoto, R. Nomura, M. Nosé, A. Fujimoto, Y. Tanaka, M. Shinohara, T. Nagatsuma, K. Shiokawa, Y. Obana, Y. Miyoshi, M. Mita, T. Takashima, and I. Shinohara, The ARASE (ERG) magnetic field investigation, *Earth, Planets and Space* **70**, 43 (2018).
- [49] Y. Miyoshi, Y. Katoh, T. Nishiyama, T. Sakanoi, K. Asamura, and M. Hirahara, Time of flight analysis of pulsating aurora electrons, considering wave-particle interactions with propagating whistler mode waves, *Journal of Geophysical Research: Space Physics* **115**, 10.1029/2009JA015127 (2010).
- [50] M. Fukizawa, T. Sakanoi, Y. Miyoshi, K. Hosokawa, K. Shiokawa, Y. Katoh, Y. Kazama, A. Kumamoto, F. Tsuchiya, Y. Miyashita, Y. M. Tanaka, Y. Kasahara, M. Ozaki, A. Matsuoka, S. Matsuda, M. Hikishima, S. Oyama, Y. Ogawa, S. Kurita, and R. Fujii, Electrostatic Electron Cyclotron Harmonic Waves as a Candidate to Cause Pulsating Auroras, *Geophysical Research Letters* **45**, 12,661 (2018).
- [51] X. Fang, C. E. Randall, D. Lummerzheim, W. Wang, G. Lu, S. C. Solomon, and R. A. Frahm, Parameterization of monoenergetic electron impact ionization, *Geophysical Research Letters* **37**, 10.1029/2010GL045406 (2010).
- [52] M. Fukizawa, T. Sakanoi, Y. Miyoshi, Y. Kazama, Y. Katoh, Y. Kasahara, S. Matsuda, A. Kumamoto, F. Tsuchiya, A. Matsuoka, S. Kurita, S. Nakamura, M. Shoji, M. Teramoto, S. Imajo, I. Shinohara, S.-Y. Wang, S. W.-Y. Tam, T.-F. Chang, B.-J. Wang, and C.-W. Jun, Statistical Study of Approaching Strong Diffusion of Low-Energy Electrons by Chorus and ECH Waves Based on In Situ Observations, *Journal of Geophysical Research: Space Physics* **127**, e2022JA030269 (2022).
- [53] J. M. Picone, A. E. Hedin, D. P. Drob, and A. C. Aikin, NRLMSISE-00 empirical model of the atmosphere: Statistical comparisons and scientific issues, *Journal of Geo-*

- physical Research: Space Physics **107**, SIA 15 (2002).
- [54] H. J. Opgenoorth, I. Hägström, P. J. S. Williams, and G. O. L. Jones, Regions of strongly enhanced perpendicular electric fields adjacent to auroral arcs, *Journal of Atmospheric and Terrestrial Physics The Fourth International EISCAT Workshop*, **52**, 449 (1990).
- [55] B. S. Lanchester, K. Kaila, and I. W. McCrea, Relationship between large horizontal electric fields and auroral arc elements, *Journal of Geophysical Research: Space Physics* **101**, 5075 (1996).
- [56] R. A. Greenwald, Diffuse radar aurora and the gradient drift instability, *Journal of Geophysical Research (1896-1977)* **79**, 4807 (1974).
- [57] M. J. Schmidt and S. P. Gary, Density gradients and the Farley-Buneman instability, *Journal of Geophysical Research (1896-1977)* **78**, 8261 (1973).
- [58] M. Oppenheim, N. Otani, and C. Ronchi, Saturation of the Farley-Buneman instability via nonlinear electron $E \times B$ drifts, *Journal of Geophysical Research: Space Physics* **101**, 17273 (1996).
- [59] N. F. Otani and M. Oppenheim, A saturation mechanism for the Farley-Buneman instability, *Geophysical Research Letters* **25**, 1833 (1998).
- [60] J. P. St-Maurice, W. Kofman, and E. Kluzek, Electron heating by plasma waves in the high latitude E-region and related effects: Observations, *Advances in Space Research* **10**, 225 (1990).
- [61] J.-P. St-Maurice and L. Goodwin, Revisiting the Behavior of the E-Region Electron Temperature During Strong Electric Field Events at High Latitudes, *Journal of Geophysical Research: Space Physics* **126**, 2020JA028288 (2021).
- [62] M. F. Ivarsen, J.-P. St-Maurice, D. R. Huyghebaert, M. D. Gillies, F. Lind, B. Pitzel, and G. C. Hussey, Deriving the Ionospheric Electric Field From the Bulk Motion of Radar Aurora in the E-Region, *Journal of Geophysical Research: Space Physics* **129**, e2024JA033060 (2024).
- [63] K. Hosokawa, A. Kadokura, N. Sato, S. E. Milan, M. Lester, G. Bjornsson, and Th. Saemundsson, Electric field modulation behind pulsating aurora, *Journal of Geophysical Research: Space Physics* **113**, 10.1029/2008JA013601 (2008).
- [64] M. F. Ivarsen, Y. Jin, A. Spicher, W. Miloch, and L. B. N. Clausen, The Lifetimes of Plasma Structures at High Latitudes, *Journal of Geophysical Research: Space Physics* **126**, e2020JA028117 (2021).
- [65] M. F. Ivarsen, J.-P. St-Maurice, J. Park, J. Klenzing, Y. Jin, and W. Lee, Plasma Structure Decay Rates in the Equatorial Ionosphere Are Strongly Coupled by Turbulence, *Geophysical Research Letters* **51**, e2024GL109441 (2024).
- [66] R. T. Tsunoda, High-latitude F region irregularities: A review and synthesis, *Reviews of Geophysics* **26**, 719 (1988).
- [67] M. Ivarsen, Y. Jin, D. Huyghebaert, Y. Miyashita, J.-P. St-Maurice, G. Hussey, K. McWilliams, S. Kasahara, D. Sibeck, K. Song, P. Jayachandran, B. Dan, L. Clausen, S. Yokota, Y. Miyoshi, Y. Kasahara, I. Shinohara, and A. Matsuoka, Transient, Turbulent Hall Currents in the Sunlit Terrestrial Ionosphere (2024).
- [68] M. F. Ivarsen, J.-P. St-Maurice, G. C. Hussey, D. Galeschuk, A. Lozinsky, B. Pitzel, and K. A. McWilliams, An Algorithm to Separate Ionospheric Turbulence Radar Echoes From Those of Meteor Trails in Large Data Sets, *Journal of Geophysical Research: Space Physics* **128**, e2022JA031050 (2023).
- [69] T. N. Davis and M. Sugiura, Auroral electrojet activity index AE and its universal time variations, *Journal of Geophysical Research* **71**, 785 (1966).
- [70] W. Baumjohann and R. Nakamura, 5.03 - Magnetospheric Contributions to the Terrestrial Magnetic Field, in *Treatise on Geophysics (Second Edition)*, edited by G. Schubert (Elsevier, Oxford, 2007) pp. 79–90.
- [71] J. F. Vickrey, R. R. Vondrak, and S. J. Matthews, The diurnal and latitudinal variation of auroral zone ionospheric conductivity, *Journal of Geophysical Research: Space Physics* **86**, 65 (1981).
- [72] V. Coumans, J.-C. Gérard, B. Hubert, M. Meurant, and S. B. Mende, Global auroral conductance distribution due to electron and proton precipitation from IMAGE-FUV observations, *Annales Geophysicae* **22**, 1595 (2004).
- [73] P. T. Newell, T. Sotirelis, and S. Wing, Diffuse, monoenergetic, and broadband aurora: The global precipitation budget, *Journal of Geophysical Research: Space Physics* **114**, 10.1029/2009JA014326 (2009).
- [74] E. Bland, F. Tesema, and N. Partamies, D-region impact area of energetic electron precipitation during pulsating aurora, *Annales Geophysicae* **39**, 135 (2021).
- [75] J. D. Sahr and B. G. Fejer, Auroral electrojet plasma irregularity theory and experiment: A critical review of present understanding and future directions, *Journal of Geophysical Research: Space Physics* **101**, 26893 (1996).
- [76] M. M. Oppenheim, Y. Dimant, and L. P. Dyrud, Large-scale simulations of 2-D fully kinetic Farley-Buneman turbulence, in *Annales Geophysicae*, Vol. 26 (Copernicus Publications Göttingen, Germany, 2008) pp. 543–553.
- [77] B. G. Fejer and M. C. Kelley, Ionospheric irregularities, *Reviews of Geophysics* **18**, 401 (1980).
- [78] T. RGB, UCalgary Space Remote Sensing Group Data Landing Page — UCalgary SRS Data documentation (2023).